

Supporting Information - LiSCN Part I

Markus Joos^a, Maurice Conrad^{b,c}, Ashkan Rad^a, Payam Kaghazchi^d, Sebastian Bette^{a,b}, Rotraut Merkle^{*a}, Robert E. Dinnebier^a, Thomas Schleid^b, and Joachim Maier^a

a Max Planck Institute for Solid State Research, Heisenbergstr. 1, 70569 Stuttgart, Germany.

b Institut für Anorganische Chemie, University of Stuttgart, Pfaffenwaldring 55, 70569 Stuttgart, Germany.

c (present address) Institut für Photovoltaik, University of Stuttgart, Pfaffenwaldring 47, 70569 Stuttgart, Germany.

d Forschungszentrum Jülich GmbH, Institute of Energy and Climate Research, Materials Synthesis and Processing (IEK-1), 52425 Jülich, Germany.

*Corresponding author Email: r.merkle@fkf.mpg.de

Experimental

General

Anhydrous Li(SCN) is stable at air, but because of its extreme hygroscopy it has to be handled under dry inert gas or vacuum conditions. All preparations, operations, and measurements were conducted either under dry Ar or N₂ (< 1 ppm H₂O) or high vacuum (< 10⁻³ mbar). In case of electrochemical measurements, even trace amounts of water smaller than 1 ppm could cause problems, thus impedance measurements were conducted under vacuum (unless stated otherwise). Throughout this report the unit mol% will be used to indicate the degree of doping, which is defined as $n(\text{dopant})/n(\text{Li}(\text{SCN})) \cdot 100 \text{ mol\%}$, where n is the amount of substance.

Sample Preparation Undoped Li(SCN)

Synthesis

Lithium thiocyanate hydrate Li(SCN) · x H₂O (98-102 % dry basis, *Sigma-Aldrich*, Steinheim, Germany) was directly purchased and subsequently dried in a dynamic vacuum (< 10⁻³ mbar). The drying process was started at 50 °C until the melt of the hydrate solidified. The emerging solid was consequently heated to 200 °C in 20 °C steps over the course of 6 hours. To ensure dry conditions, it remained at the target temperature of 200 °C for a total of 24 hours. The result was a very hygroscopic white powder of pure Li(SCN).

Drying for Electrochemical Impedance Spectroscopy (EIS)

Every Li(SCN) sample for impedance was thoroughly dried at temperatures between 230 °C and 250 °C under high vacuum (< 10⁻³ mbar). The drying was directly conducted in the EIS measurement cell in which the sample was already contacted by platinum electrodes, and monitored by EIS over the course of at least 2-3 days. This rigorous, yet necessary drying

procedure explains the discrepancy between the here reported conductivities of anhydrous, undoped Li(SCN) compared to a previous study (Figure S13).¹

Pellet Preparation

Compacted pellets for electrochemical measurements were produced by uniaxial pressing in hardened steel dies. Cold pressing was deduced to be the most efficient compaction method for this material. With a general pellet diameter and thickness of 6 and 2.5 mm, the optimum pressing force was 15 kN (5.2 kbar) to produce on average 89 % dense pellets determined by mass and volume. A minimum pressure of 3.5 kbar had to be used to achieve sufficiently dense pellets, which were on average 86 % dense. Smaller pressures yielded densities < 80 %. Higher pressures of up to 18 kbar did not improve the density significantly. In general, pellets were pressed with thicknesses between 1.0-4.0 mm, however, thicknesses of up to 16 mm were achievable. Occasionally, the pellets were polished with Al₂O₃ lapping paper (9MIC, 3M *Lapping Film*) on the sides to remove any residue from the pressing tools.

Various, yet unsuccessful sintering procedures were attempted to improve the density further:

- heating with 5 °C/min to 80 °C, dwell for 12 h, cooling with 10 °C/min
- heating with 10 °C/min to 150 °C, dwell for 12 h, cooling with 10 °C/min
- heating with 1 °C/min to 180 °C, dwell for 12 h, cooling with 10 °C/min
- heating with 10 °C/min to 200 °C, dwell for 12 h, cooling with 10 °C/min

The sintering was done under vacuum ($\sim 10^{-6}$ mbar) in glassy-carbon crucibles (*SIGRADUR® G*) inside flame sealed silica ampoules. The pellets were surrounded and covered with additional Li(SCN) powder. Nevertheless, depending on the temperature, the white powder / pellets could turn brown, grey or even black.

Another attempted densification method was uniaxial hot-pressing (*P/O/WEBER*, Germany). The material was pressed with a 5 mm hardened steel die under 13 kN (6.6 kbar), 15 kN (7.6 kbar) or 25 kN (12.7 kN) of force and heated to 110 °C, 130 °C or 180 °C for 12 h. However, this method was inferior to cold pressing, since the obtained pellet densities were comparable to those of cold pressed ones, and the pellet would stick to the inside of the pressing die and could not be recovered unscathed.

Li(SCN) single crystals or re-crystallized melts were also thought to be suitable for conductivity measurements. Li(SCN) powder was melted in a glassy-carbon crucible (typically heated to 350 °C) and then either slowly cooled (1 °C/h) to 100 °C (in a silica ampoule under vacuum in a furnace) or quenched quickly to room temperature (in a glove box on a hot-plate). Neither method produced single crystals, and the obtained crystallites were very porous with densities < 80 %.

Sample Preparation Doped Li(SCN)

Synthesis and Preparation of Dopants

Co(SCN)₂ (99.9 %, Aldrich), Li₂S (99.98 %, Sigma-Aldrich) and Li₂(SO₄) (99.99 %, Sigma-Aldrich) were purchased from the respective manufacturer and could be directly used without any further treatment. Mg(SCN)₂ · 4 H₂O (its anhydrous state is as of yet unknown) was synthesized with cation exchange according to the procedure described in reference 2. Zn(SCN)₂ was synthesized according to literature.³ 2 g of Ba(OH)₂ · 8 H₂O (≥ 98 %, Roth) were mixed with the stoichiometric amount of NH₄(SCN) (99.99 %, Sigma-Aldrich) and dissolved in ~110 ml of deionized H₂O. The solution remained turbid despite stirring at 50 °C for ~1.5 h. About 50 ml of methanol (CH₃OH, ≥ 99.9 % p.a., Roth) were added to improve the solubility and the temperature was increased to 75 °C (0.5 h) and 80 °C (1 h), yet the cloudiness remained. Afterwards a stoichiometric amount of Zn(SO₄) · H₂O (99 %, Acros Organics) was added and Ba(SO₄) instantly precipitated. The solution was vacuum filtered. After cooling the solution in an ice bath, remaining Ba(SO₄) was again removed by a second filtration. The mixture of water and methanol was distilled off with a rotary evaporator and a white (slightly yellow) powder precipitated, which was fully dried at the Schlenk line. XRPD revealed traces of remaining Ba(SCN)₂, which were removed by re-dissolving the precipitated powder in deionized water and titration with a saturated solution of Zn(SO₄), until no more Ba(SO₄) precipitated. Anhydrous Zn(SCN)₂ was reported to crystallize in two polymorphs (α-phase with blue and β-phase with green luminescence).⁴ However, only the crystal structure of β-Zn(SCN)₂ has been reported so far,⁵ and as can be seen in Figure S5a, it does not match with the here obtained sample. A reference XRPD pattern for Zn(SCN)₂ from the New Jersey Zinc Company matches with the main peaks,⁶ supporting that Zn(SCN)₂ was successfully synthesized. The IR spectrum in Figure S5b confirms the presence of the (SCN)⁻ anion, yet some additional peaks from a contaminant are also observed. Considering the results from ICP-OES,⁷ the synthesized sample of Zn(SCN)₂ has a small contamination of Zn(SO₄) hydrates, which however does not interfere with the doping experiments.

Doping Procedure

Doping was conducted by thoroughly mixing anhydrous Li(SCN) with the doping agent, pressing the powder into a pellet with the same method as for undoped Li(SCN) and then heating the pellet stepwise to either 230 or 250 °C under high vacuum (< 10⁻³ mbar). The estimated densities of doped pellets were comparable to those of undoped material.

In case of Mg²⁺-doping, the pellet consisting of an intimately mortar-ground mixture of Li(SCN) and Mg(SCN)₂ · 4 H₂O had to be heated up slowly in a stepwise fashion, to first remove the crystal water and avoid the formation of hydroxides or oxides. Mg(SCN)₂ · 4 H₂O melts at 144 °C and decomposes at 167 °C.² To avoid any liquefaction and remove H₂O first, the pellets were heated stepwise to 80 °C, 100 °C, 120 °C, 150 °C, 180 °C and 230 °C under high vacuum directly in the EIS measurement cell. The dwell time at each temperature step was typically at least 2-3 h, monitored by measuring the impedance. At 230 °C the sample was fully dried

as described for undoped Li(SCN). Mg²⁺-doped samples were dried and measured only up to 230 °C, and a homogeneous Mg²⁺-distribution was assumed.

The thermal properties of Zn(SCN)₂ and Co(SCN)₂ were investigated by DSC as well as by visual inspection.⁷ In case of Zn(SCN)₂, the material does not change shape or color up to 200 °C, only after heating to 300 °C it expanded in volume and turned black-brown. It can therefore be concluded that Zn(SCN)₂ starts to decompose at 201 °C. It is unclear what the other peaks at lower temperatures observed in the DSC measurement correspond to (possibly a contaminant or the α- to β-phase transition). In contrast, Co(SCN)₂ did not show any signs of melting or decomposition until 333 °C. The doping procedure for both Zn(SCN)₂ and Co(SCN)₂ required less temperature steps as compared with Mg(SCN)₂ · 4 H₂O, since both could be obtained in their anhydrous forms:

Zn(SCN)₂: 25 °C → 130 °C → 150-170 °C → 190 °C → 230-250 °C

Co(SCN)₂: 25 °C → 150 °C → 200 °C → 250 °C

At 250 °C the sample was dried with the above described procedure. The entire process was monitored by EIS in the same way as described for Mg²⁺-doping. Dwell times on each temperature step varied between 1.5 h and >100 h. Acceptor doping with Li₂S and Li₂(SO₄) was attempted, either by the same method as for donor doping or by co-precipitation after melting, but was ultimately unsuccessful (Figure S13b).

Synthesis of Mg_{1+x}Li_{4-2x}(SCN)₆ (x = 0.02)

Doping beyond the solubility limit of Mg²⁺ in Li(SCN) (about 3-5 mol%) lead to the formation of Mg_{1.02}Li_{3.96}(SCN)₆. The synthesis procedure was basically the same as the doping procedure with Mg(SCN)₂ · 4 H₂O, although the stepwise heating was done slower and with more steps. Even though a mixture of 80 mol% Li(SCN) and 20 mol% Mg(SCN)₂ (i.e. 100 mol% and 25 mol%) should be appropriate to produce Mg_{1.02}Li_{3.96}(SCN)₆, it was observed multiple times that the effectively available amount of Mg(SCN)₂ for the synthesis was reduced.⁷ Possibly volatile decomposition products of Mg(SCN)₂ · 4 H₂O formed, which vaped off during the synthesis under vacuum, and unreacted Li(SCN) remained. However, by using an excess of Mg(SCN)₂ · 4 H₂O (up to 60 mol%), eventually an additional, unknown phase was observed to form. Numerous attempts to produce a pure phase sample of Mg_{1.02}Li_{3.96}(SCN)₆ were unsuccessful, including various heating and cooling cycles with different rates, longer synthesis times (up to 44 days), higher temperatures (up to 270 °C) and using a different precursor (Mg(SCN)₂ · 4 THF, an adduct with tetrahydrofuran).² Although a nominal amount of 25 mol% Mg(SCN)₂ (i.e. relative ratio of 80 mol% Li(SCN) and 20 mol% Mg(SCN)₂) should be appropriate to synthesize the new phase, the highest achieved purity of ~81 wt.-% according to Rietveld refinement (Figure S1) was obtained by using an excess of 35 mol% Mg(SCN)₂ (i.e. 60 mol% in Figure 1b). Since the employed tetrahydrate of Mg(SCN)₂ can decompose during heating,² possibly amorphous and volatile decomposition products were formed during synthesis, which could influence the stoichiometric ratio.

X-Ray Powder Diffraction (XRPD)

To confirm the retention of phase purity after heat treatments, doping, or other procedures, XRPD patterns were recorded in a Bragg-Brentano configuration at room temperature (*PANalytical* Empyrean Series 2 diffractometer, Cu-K $_{\alpha 1}$, 40 kV, 40 mA, PIXcel 3D detector, $2\theta = 10^\circ$ - 90°) and analysed with the *PANalytical* HighScore Plus software (Version 3.0e). The samples were measured either in sealed borosilicate glass capillaries (0.5 or 0.7 mm diameter, *Hilgenberg* glass no. 14) or in a polycarbonate dome (*PANalytical*) under Ar atmosphere.

XRPD patterns for detailed analyses and refinement were collected at room temperature on a laboratory powder diffractometer in Debye-Scherrer geometry (Stadi P-Diffraktometer *Stoe*, Cu-K $_{\alpha 1}$ radiation from primary Ge(111)-Johann-type monochromator, triple array of Mythen 1 K detectors *Dectris*). Samples were sealed in capillaries as described above and spun during the measurement. The pattern was measured in a 2θ range from 0° to 110° applying a total scan time of 30 minutes.

Temperature dependent *in situ* X-ray diffraction experiments on Li(SCN) and Li(SCN) – Mg $_{1.02}$ Li $_{3.96}$ (SCN) $_6$ composites were performed on a D8-Advance diffractometer (*Bruker*, Cu-K $_{\alpha 1}$ radiation from primary Ge(111)-Johann-type monochromator, Lynx Eye position sensitive detector (*Bruker*)) in Debye-Scherrer geometry using a water cooled furnace (mri capillary heater, 25-1000 °C) for heating the capillary.⁷ For the respective temperature ranges, Li(SCN) – Mg $_{1.02}$ Li $_{3.96}$ (SCN) $_6$ composites could be measured in glass capillaries, yet Li(SCN) had to be filled in fused silica (0.5 mm) to avoid fracture of the capillary. XRPD patterns of Li(SCN) were collected in a 2θ range from 5° to 40° applying a total scan time of 2 h. The patterns were recorded in 20 K steps and in 5 K steps close to the melting point. Prior to each measurement a delay time of 10 minutes was applied in order to ensure thermal equilibrations. XRPD patterns of Li(SCN) – Mg $_{1.02}$ Li $_{3.96}$ (SCN) $_6$ composites were collected in a 2θ range from 5° to 90° applying a total scan time of 6 h.

Crystal Structure Solution

The program TOPAS 6.0 was used to determine and refine the crystal structure of Mg $_{1.02}$ Li $_{3.96}$ (SCN) $_6$.⁸ Indexing of the phases was carried out by an iterative use of singular value decompositions (LSI)⁹ leading to a *F*-centered cubic unit cell with $Fd\bar{3}m$ as most probable space group derived from systematic absences of reflections. The peak profile and the precise lattice parameters (Table S1) were determined by LeBail¹⁰ applying the fundamental parameter approach of TOPAS.^{11,12} The background was modelled by employing Chebychev polynomials of 6th order, the refinement converged quickly. During the refinement, the presence of additional peaks attributed to Li(SCN) was observed. Hence, the crystal structure of Li(SCN) was included into the refinement,¹³ and into the subsequent process of crystal structure determination.

The crystal structure was solved by applying the global optimization method of simulated annealing (SA) in real space as implemented in TOPAS.¹⁴ The exact phase composition was unknown prior to the crystal structure solution. Hence different sets of magnesium, lithium

and thiocyanate ions were used for the structure solution and the global optimization was carried out multiple times. The thiocyanate anions were described by rigid bodies in z-matrix notation and rotated and translated freely through the unit cell. Atoms situated on identical or special positions were identified by using a merging radius of 0.7 Å.¹⁵ Within the unit cell, only one crystallographically independent thiocyanate anion was found on the special position 48*f*. Two magnesium cations were localized on an 8*a* and 16*d* special position. A detailed inspection of the difference Fourier map indicated an occupational magnesium-lithium disorder at the 16*d* position. Some additional residual electron density was found on a 32*e* special position pointing to a partially occupied lithium site. During the final refinement, the occupancy of this site was constrained to the occupancies of the positional disordered 16*d* cation position in order to maintain charge balance. The resulting composition was determined as $\text{Mg}_{1+x}\text{Li}_{4-2x}(\text{SCN})_6$ with $x = 0.02$, hence close to $\text{MgLi}_4(\text{SCN})_6$. The final Rietveld refinement led to reasonable agreement factors (Table S1) and a good graphical result of the fit (Figure S1).¹⁶ Selected crystallographic data, bond lengths and angles are given in Table S2 and S3. The crystallographic dataset was deposited in the CCDC database under the deposition number: 2152204.

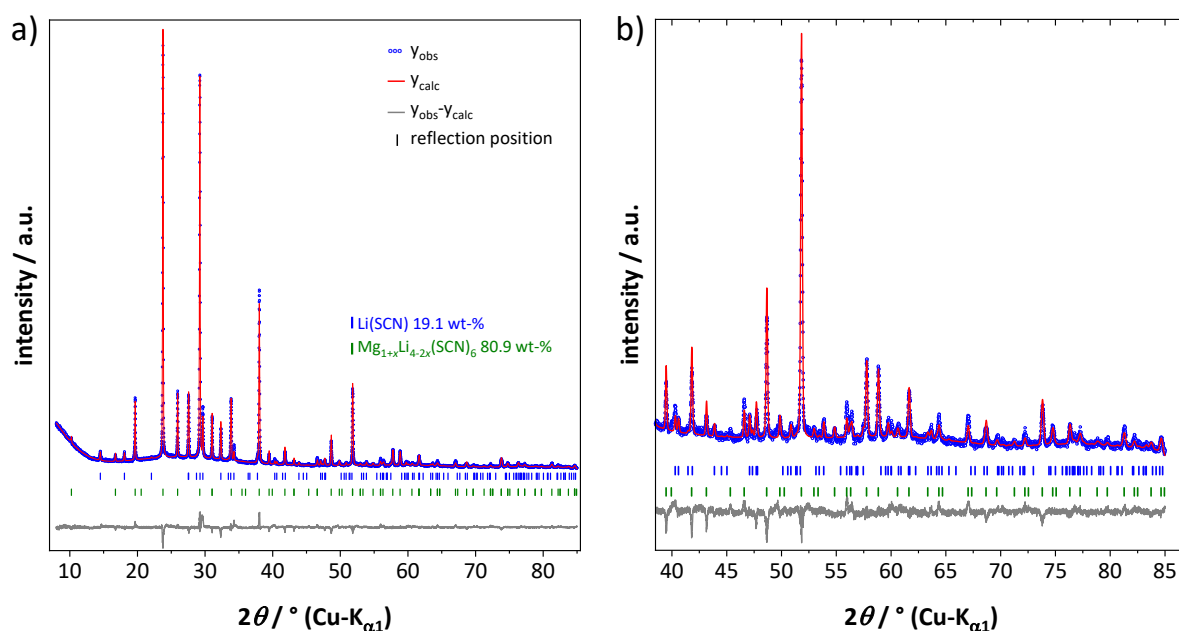


Figure S1: a) Final Rietveld refinement of $\text{Mg}_{1+x}\text{Li}_{4-x}(\text{SCN})_6$, and b) magnification of the high angle region for clarity.

Table S1: Crystallographic and Rietveld refinement data of $\text{Mg}_{1+x}\text{Li}_{4-2x}(\text{SCN})_6$ with $x = 0.02$.

compound name	magnesium lithium isothiocyanate
molecular formula	$\text{Mg}_{1+x}\text{Li}_{4-2x}(\text{SCN})_6$ with $x = 0.02$
sum formula	$\text{C}_6\text{Li}_{3.96}\text{Mg}_{1.02}\text{N}_6\text{S}_6$
molecular weight / g · mol⁻¹	401.01
temperature / K	328
space group	$Fd\bar{3}m$ (no. 227)
Z	8
a / Å	14.9612(2)
V / Å³	3348.9(2)
ρ_{calc} / g · cm⁻³	1.59
wavelength / Å	1.5406
R-p / %^{a)}	5.05
R-wp / %^{a)}	6.33
R-F² / %^{a)}	4.50
no. of variables	40

^{a)}R-p, R-wp and R-F² as defined in TOPAS (Bruker AXS).

Table S2: Atomic coordinates of $\text{Mg}_{1+x}\text{Li}_{4-2x}(\text{SCN})_6$ with $x = 0.02$ at 55 °C.

Atom	Wyckoff site	Symmetry	S.O.F.	x	y	z	B _{eq} / Å ²
Mg(1)	8a	$\bar{4}3m$	1	0	0	0	5.0(1) ^{a)}
Li(2)			0.979(6)				5.0(1) ^{a)}
Mg(2)	16d	$\bar{3}m$	0.021(6)	5/8	5/8	5/8	5.0(1) ^{a)}
Li(3)	32e	.3m	0.459(6)	0.3704(8)	0.3704(8)	0.3704(8)	5.0(1) ^{a)}
S(1)	48f	2.mm	1	0.3283(4)	0	0	5.0(1) ^{a)}
C(1)	48f	2.mm	1	0.2184(3)	0	0	5.0(1) ^{a)}
N(1)	48f	2.mm	1	0.1413(2)	0	0	5.0(1) ^{a)}

^{a)}one global parameter for the B_{eq} of all sites was defined.

Table S3: Selected bond distances and angles of $\text{Mg}_{1+x}\text{Li}_{4-2x}(\text{SCN})_6$ with $x = 0.02$ at $55\text{ }^\circ\text{C}$.

Atoms	Distance / Å	Atoms	Angles / °
Mg(1)-N(1)	$6 \times 2.113(2)$	N(1)-Mg(1)-N(1)	90
Li/Mg(2)-S(1)	$6 \times 2.736(1)$	S(1)-Li/Mg(2)-S(1)	83.214(1), 96.786(1)
Li(1)-N(1)	$3 \times 2.567(13)$	N(1)-Li(3)-S(1)	176.1(1), 183.1 (1), 104.1(1)
Li(1)-S(1)	$3 \times 2.813(13)$	N(1)-Li(3)-N(1)	71.2(3)
Mg(1)-Mg(1)	$4 \times 6.4784(1)$	S(1)-Li(3)-S(1)	80.4(3)

Infrared (IR) Spectroscopy

IR spectroscopy was performed on an ALPHA II FT-IR (Fourier transform) spectrometer from Bruker Optik GmbH with an attenuated total reflection (ATR) unit in an argon filled glove box. Prior to the measurement, the powder was thoroughly ground in an agate mortar.

Inductively Coupled Plasma Atomic Emission Spectroscopy (ICP-OES)

Samples of doped Li(SCN) and composites of Li(SCN) and $\text{Mg}_{1.02}\text{Li}_{3.96}(\text{SCN})_6$ were either directly dissolved in double-distilled water under neutral conditions or 5 vol.-% HNO_3 (65 %) were added. The measurements were performed on a Spectro Ciros ICP-OES spectrometer (Spectro Analytical Instruments GmbH, Germany).

Electrochemical Impedance Spectroscopy (EIS)

Compacted pellets were DC-sputtered in a glove box (Emitech K575X, 100 mA current, 4 min sputter time) on both sides with ~ 400 nm ruthenium (99.95 %, Lesker). For measurements, in which the temperature did not exceed $270\text{ }^\circ\text{C}$, the pellets were mounted into a silica holder with a silica rod and the ruthenium sides were contacted under slight pressure with platinum electrodes. All measurement cells were leak-checked with a helium leak detector (UL 200 dry, Oerlikon Leybold Vacuum).

The equilibration time at each temperature step was typically set to 1 h. Impedance spectra were recorded on a Novocontrol Alpha-A analyzer (two-wire measurement) between 10^6 to 10^{-2} Hz and a 0.1 V amplitude. At least two spectra with a 1 h delay were acquired at each condition to confirm reproducibility. If necessary, the stray impedance of the set-up (measured separately by short-circuiting the electrodes) was pointwise subtracted.

Fitting of the impedance spectra was done with Zview (Scribner, Version 3.5.c) by equivalent circuits consisting of resistors, constant phase elements (CPE) and / or capacitors. Conductivities σ and dielectric constants ϵ_r were extracted using $\sigma = L/(R \cdot A)$ and $\epsilon_r = (C_{\text{eff}} \cdot L)/(\epsilon_0 \cdot A)$, in which R is resistance, L is sample thickness, A is electrode area, ϵ_0 is the electrical permittivity of free space, and C_{eff} is the effective capacitance calculated from

$C_{\text{eff}} = Q^{n-1} \cdot R^{(n-1)}$ ($n = 1$ for capacitors), where Q and n are the magnitude and exponent of a CPE.¹⁷

Direct Current (DC) Measurements

DC measurements were conducted under constant current with lithium irreversible (ruthenium, 99.95 %, *Lesker*) electrodes (Figure S8a and S11, same preparation as for EIS) or under open circuit voltage (OCV) condition with lithium reversible (Li metal 99.9 %, *Alfa Aesar*, and LiAl > 99.5 %, *ELSAindustries SAS*) electrodes (Figure S8b). In the first case, the sample was prepared and measured in the same way as described for sample preparation and EIS measurements. In case of lithium reversible electrodes, LiAl powder was uniaxially co-pressed with freshly dried Li(SCN) (5 mm pressing die, force of 10 kN), and a 5 mm punched Li metal disk was pressed on top of the other side with a hand-crank in the same set-up. Molybdenum disks were put in between the lithium containing electrodes and the platinum contacts (cell arrangement; Pt-Mo-Li | Li(SCN) | LiAl-Mo-Pt) to prevent the formation of lithium alloys. Voltage and current were measured and monitored with a potentiostat (*Keithley*, 2400 Sourcemeter).

Density Functional Theory (DFT) Calculations

DFT calculations were performed using the Vienna ab initio simulation package (VASP)^{18,19} with the projector augmented wave pseudopotential approach.^{20,21} The PBE exchange-correlation functional²² was used. The convergence criteria for electronic self-consistency and geometry steps were 10^{-5} eV and 10^{-4} eV/Å. All calculations were spin-polarized with an energy cutoff of 500 eV for the plane wave basis sets. Atomic geometry relaxation was performed simultaneously with the cell optimization (ISIF = 3). Sampling of the Brillouin zone was performed using a $2 \times 2 \times 2$ k -point mesh. After full DFT-PBE relaxation, the Li(SCN) $1 \times 1 \times 1$ unit cell had the following lattice parameters: $a = 12.98766$ Å, $b = 3.68167$ Å, $c = 5.31050$ Å. A fully relaxed $1 \times 4 \times 3$ supercell was employed for all defect chemical and Climbing Image Nudged Elastic Band (CI-NEB) calculations.

The energies for Schottky and Frenkel defect formation were calculated for the respective defect pairs in neutral supercells. The Supercell program²⁵ was used to create possible configurations using the permutation theory by distributing ions with partial occupancy among the empty sites and calculating Coulomb interactions using the Ewald summation method. The Schottky defect pair was obtained from DFT calculations for 15 favorable structures according to the electrostatic analysis from the Supercell program. These 15 structures have the minimum electrostatic energy among all possible combinations obtained from the Supercell program. The Frenkel pair defective structure was modelled by considering the most favorable interstitial- and vacancy-containing structures. The lowest energies for a Schottky defect pair ($V_{\text{Li}} + V_{\text{SCN}}$, 0.34 eV Figure S2a) and Frenkel defect pair ($\text{Li}_i + V_{\text{Li}}$, 1.1-1.2 eV Figure S2b and c) show that the most favorable intrinsic defect in Li(SCN) is the Schottky pair. For both defect pairs, configurations with the oppositely charged defects being close to

each other are lower in energy than with distant defects, in line with the experimentally observed tendency in Li(SCN) for defect association.

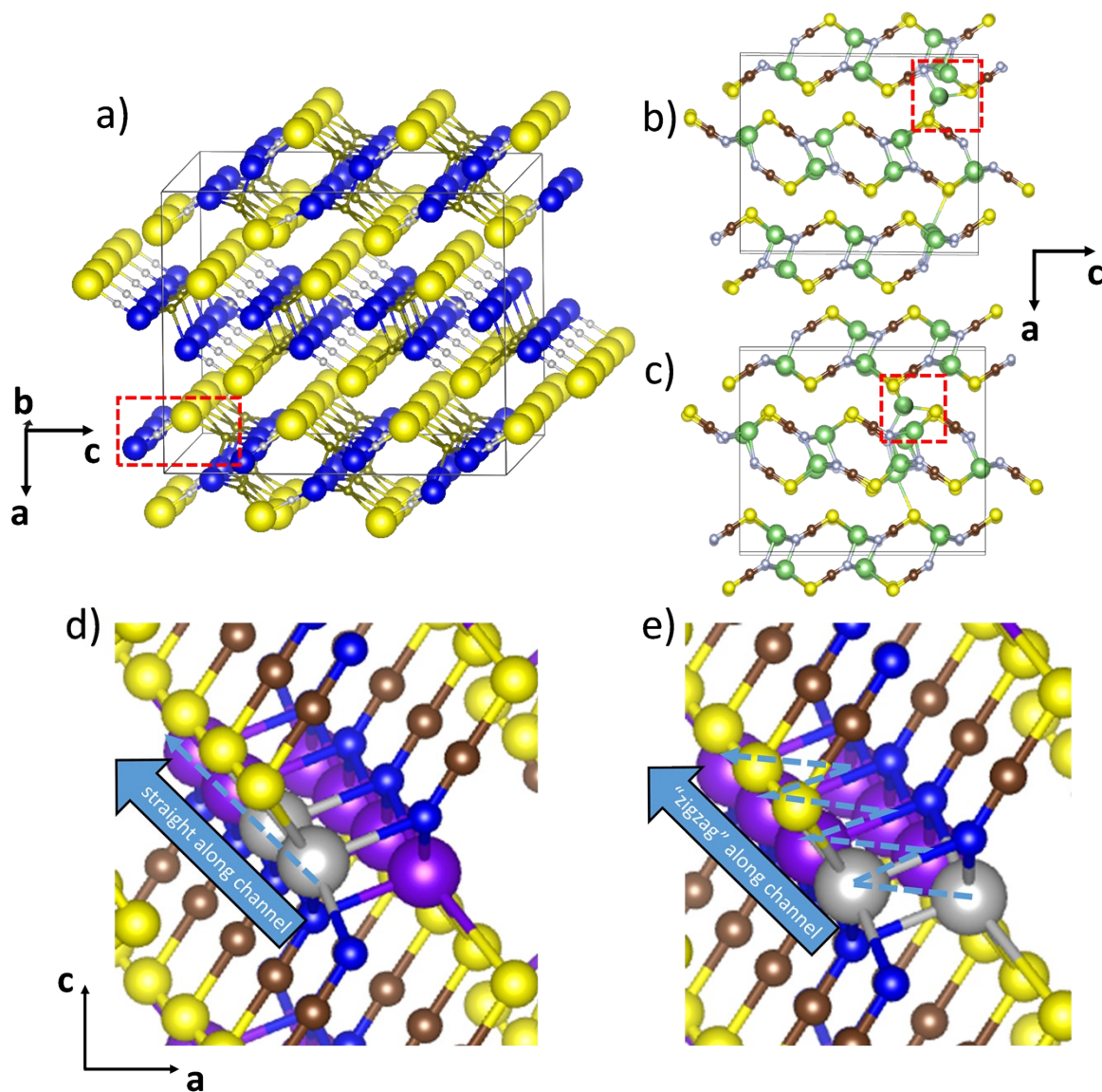


Figure S2: Li(SCN) supercells used in the DFT calculations of the formation energies (enthalpies) for a) a Schottky defect pair (0.34 eV), and a Frenkel defect pair with b) 1.2 eV and c) 1.1 eV. The loci of the defects are marked with red dashed rectangles. d) Straight V_{Li}^{\cdot} migration path along *b* direction, e) "zigzag" path via the shortest distances between regular Li sites. S indicated by yellow spheres, Li cations are indicated by silver/violet color in a),d),e), and green in b),c).

Defect migration barriers were calculated by the CI-NEB scheme using 9 intermediate images. For the case of V_{Li}^{\cdot} migration, a cell with a single Li vacancy could be used (the charge of the V_{Li}^{\cdot} is compensated by an electron hole of delocalized character – the cell geometry does not show any characteristics of a localized electronic defect). A straight path along *b* direction (Figure S2c, 0.26 eV) and a "zigzag" path via the shortest distances between regular Li sites

(Figure S2d, 0.08 eV) were explored. For comparison, the "zigzag" barrier was also calculated in a charged supercell where a jellium background charge compensates the Li vacancy – this yielded almost the same barrier height (0.28 eV) as the neutral cell. For Li_i^{\cdot} , a supercell containing a Frenkel pair with large distance between Li_i^{\cdot} and $\text{V}_{\text{Li}}^{\cdot}$ was used moving only the Li_i^{\cdot} (attempts to use a single Li_i^{\cdot} with electronic compensation led to localized electronic defects recognized from individual distorted thiocyanate anions). The Li_i^{\cdot} barrier along b direction amounts to 0.88 eV, indicating that lithium interstitials are not only disfavored by a high formation energy but also have a high migration barrier.

Material Characterizations and Structure Determination

$\text{Mg}_{1.02}\text{Li}_{3.96}(\text{SCN})_6$ crystallizes in a cubic unit cell $Fd\bar{3}m$ ($Z = 8$) with a large volume ($3348.9(2) \text{ \AA}^3$), in which all cations exhibit an octahedral coordination (Figure S3). The Mg^{2+} cation is situated at the origin of the unit cell on an $8a$ special position in a $\text{Mg}(\text{NCS})_6$ octahedron ($(\text{SCN})^-$ parallel to the octahedron's axes, Figure S3a). One Li^+ cation is situated on a $16d$ special position in a $(\text{Li/Mg})(\text{SCN})_6$ octahedron ($(\text{SCN})^-$ orthogonal to the octahedron's axes, Figure S3b), which shows minor mixed occupancy with magnesium (2.1 %), and leads to a flexible phase composition of $\text{Mg}_{1+x}\text{Li}_{4-2x}(\text{SCN})_6$ with $x = 0.02$. Another Li^+ cation was found on a $32e$ special position in a $\text{Li}_{1-y}\square_y(\text{NCS})_3(\text{SCN})_3$ octahedron (Figure S3c), for which the site occupancy is ≤ 0.5 due to electroneutrality and the mixed Li-Mg-occupation of the $16d$ site. Since the Li-N and Li-S distances are rather high ($2.57(2) \text{ \AA}$ and $2.81(2) \text{ \AA}$), the $32e$ site can be regarded as an interstitial cation position. In case of the $(\text{SCN})^-$ anion, the nitrogen atom is coordinated in $[\text{N}(\text{Mg})(\text{Li}_{1-y}\square_y)_2]$, and the sulfur atom in $[\text{S}(\text{Li/Mg})_2(\text{Li}_{1-y}\square_y)_2]$ (Figure S3d).

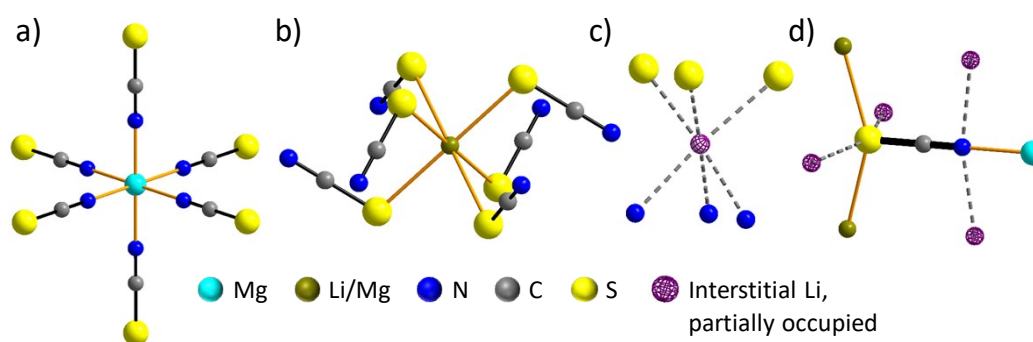


Figure S3: Coordination spheres of the cations and anions in the crystal structure of $\text{Mg}_{1.02}\text{Li}_{3.96}(\text{SCN})_6$.

The interstitial, partially occupied $\text{Li}_{1-y}\square_y(\text{NCS})_3(\text{SCN})_3$ octahedron ($y \leq 0.5$) is face-sharing with one $\text{Mg}(\text{NCS})_6$ octahedron and corner-sharing with two $(\text{Li/Mg})(\text{SCN})_6$ octahedra (Figure S4a). In the crystal structure of $\text{Mg}_{1.02}\text{Li}_{3.96}(\text{SCN})_6$, there is another interstitial octahedral void (Figure S4b) situated at $\frac{1}{2}, \frac{1}{2}, \frac{1}{2}$ on an $8b$ position. This void is exclusively coordinated by six thiocyanate-related sulfur atoms $\square(\text{SCN})_6$, and its coordination polyhedron shares faces with four $(\text{Li/Mg})(\text{SCN})_6$ and four $\text{Li}_{1-y}\square_y(\text{NCS})_3(\text{SCN})_3$ octahedra (Figure S4b). The face-sharing

connectivity of neighboring $(\text{Li/Mg})(\text{SCN})_6$ and $\square(\text{SCN})_6$ octahedra could indicate possible migration paths of mobile defects through the lattice (Figure S4c and d).

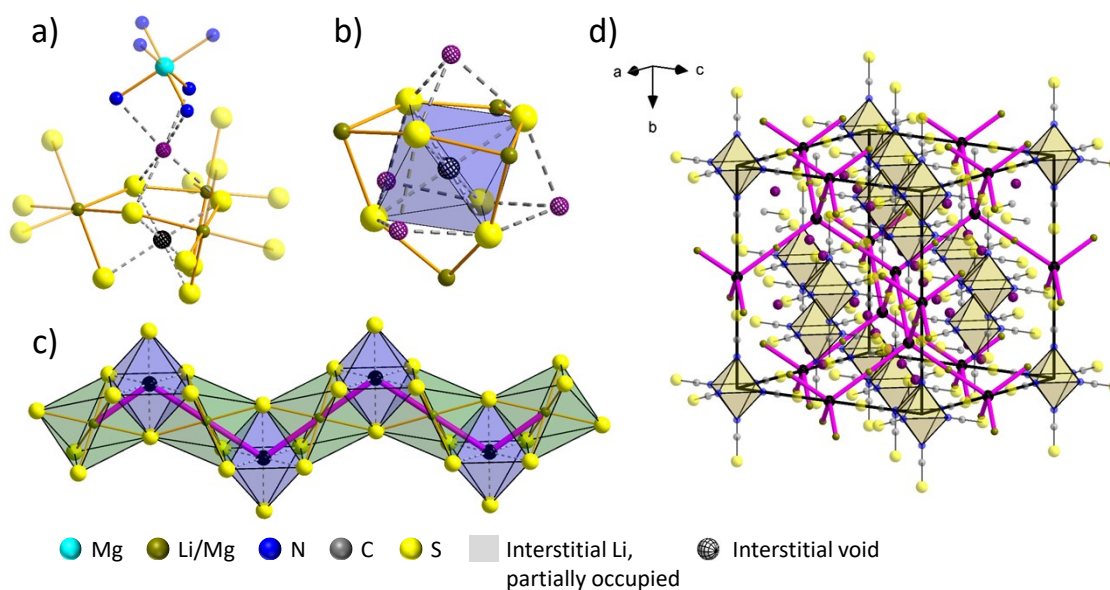


Figure S4: Octahedral coordination spheres of a) interstitial, partially occupied $\text{Li}_{1-y}\square_y(\text{NCS})_3(\text{SCN})_3$ and b) interstitial voids $\square(\text{SCN})_6$. c) Chain of face-sharing $(\text{Li/Mg})(\text{SCN})_6$ (green) and $\square(\text{SCN})_6$ (blue) octahedra providing a potential migration path of mobile defects (magenta bonds). d) 3D network of potential migration paths (magenta bonds) in the unit cell of $\text{Mg}_{1.02}\text{Li}_{3.96}(\text{SCN})_6$ ($\text{Mg}(\text{NCS})_6$ octahedra are presented in yellow).

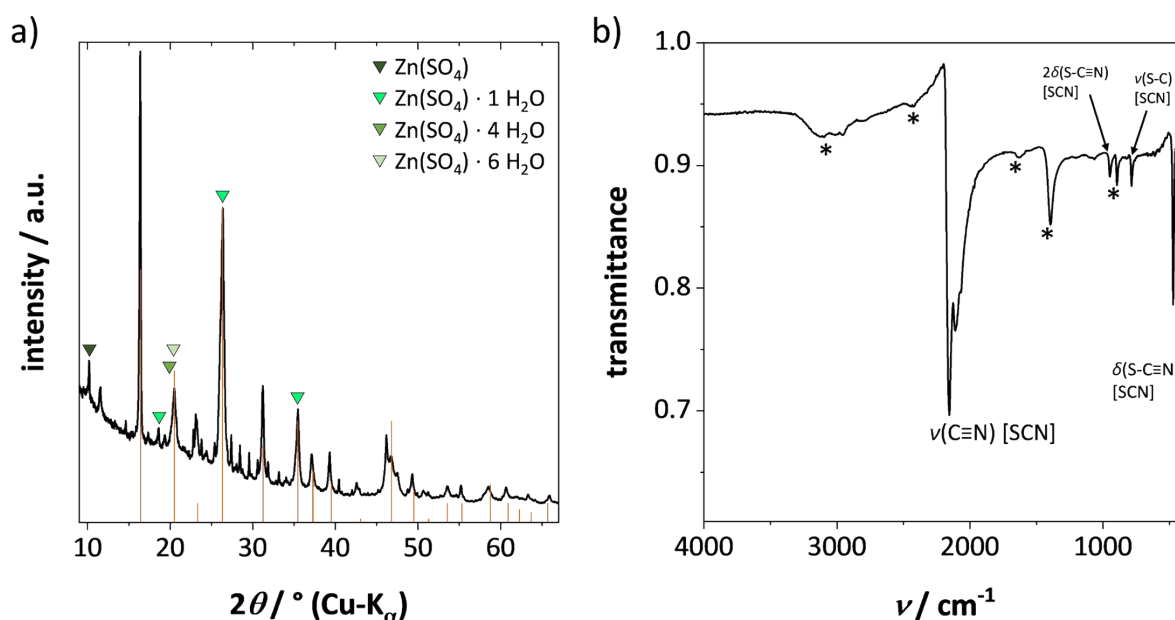


Figure S5: a) XRPD pattern of $\text{Zn}(\text{SCN})_2$ with an inserted reference pattern (red bars) from literature.⁶ Small amounts of contaminant side phases are indicated. b) IR spectrum of synthesized $\text{Zn}(\text{SCN})_2$. Besides the well-known $(\text{SCN})^-$ bands,¹³ additional signals in the IR

spectrum are marked with an asterisk. Considering the results from XRPD in (a), as well as SEM-EDX and ICP-OES,⁷ the additional bands can be attributed to small amounts of Zn(SO₄) hydrates.²⁸

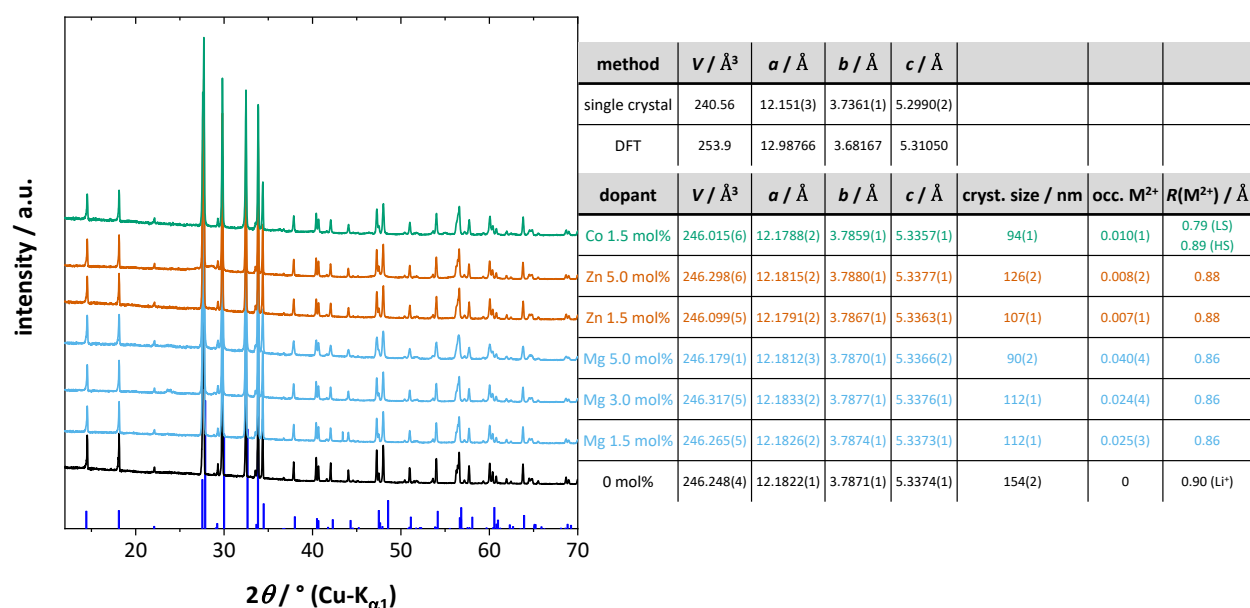


Figure S6: XRPD patterns of undoped (black), Mg²⁺-doped (blue), Zn²⁺-doped (red) and Co²⁺-doped (green) Li(SCN). The table on the right compares the structure data from Rietveld refinement with single crystal data from literature (blue bars in the diffractogram)¹³ and from DFT calculation. The last column in the table lists the respective ionic radii.²⁹

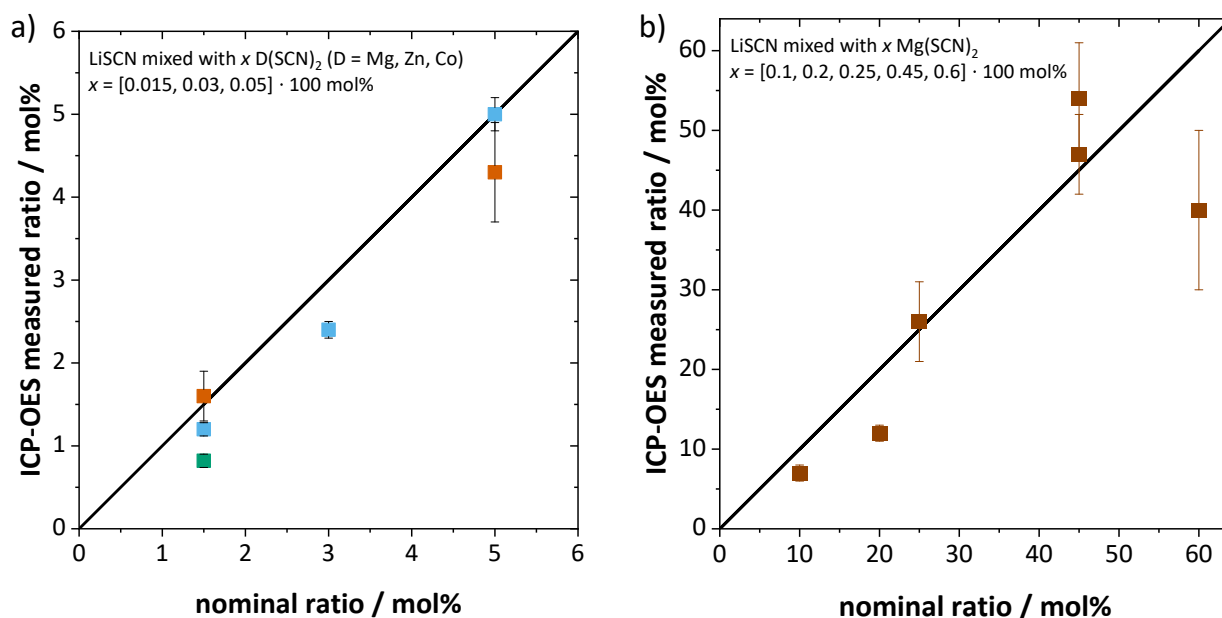


Figure S7: ICP-OES results of different Li(SCN)-D(SCN)₂ (D = Mg, Zn, Co) samples after heat and vacuum treatment, showing samples a) within (Mg blue, Zn red, Co green) and b) beyond (Mg dark red) the donor dopant solubility limit of Li(SCN).

Electrochemical Measurements

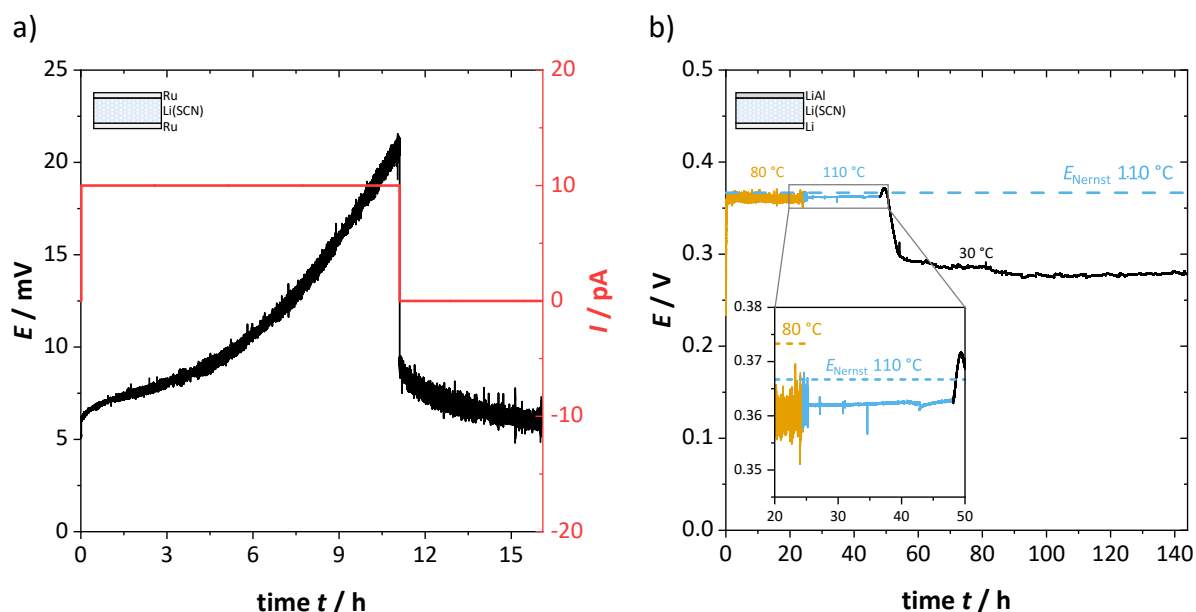


Figure S8: a) Galvanostatic DC polarization measurement of undoped Li(SCN) with Li-irreversible ruthenium electrodes at 30 °C in 100 sccm N₂ flow. The continuous increase in voltage (i.e. polarization) shows the blocking nature of ruthenium electrodes versus lithium insertion. b) Electromotive force measurement (EMF) under open circuit voltage (OCV) condition with Li and LiAl as reference electrodes in 100 sccm Ar flow. The Nernst voltage at 80 °C (orange, dashed line) and 110 °C (blue, dashed line) was calculated according to Wen et al.³⁰

The Nernst voltage shown in Figure S8b was calculated with the equation:³⁰

$$E_{\text{Nernst}} = (451 - 0.220 \cdot T/\text{K}) \text{ mV} \quad (1)$$

for the respective temperature. The transference number $\langle t_{\text{Li}^+} \rangle$ was then obtained using the well-known relation $E = E_{\text{Nernst}} \cdot \langle t_{\text{Li}^+} \rangle$, yielding values of $\langle t_{\text{Li}^+} \rangle \geq 0.99$.

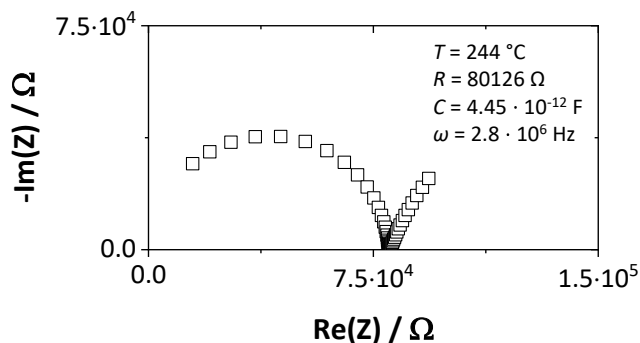


Figure S9: Exemplary impedance spectrum of undoped Li(SCN) with Li⁺ blocking ruthenium electrodes at higher temperatures (244 °C) showing the expected Warburg-type low frequency response.

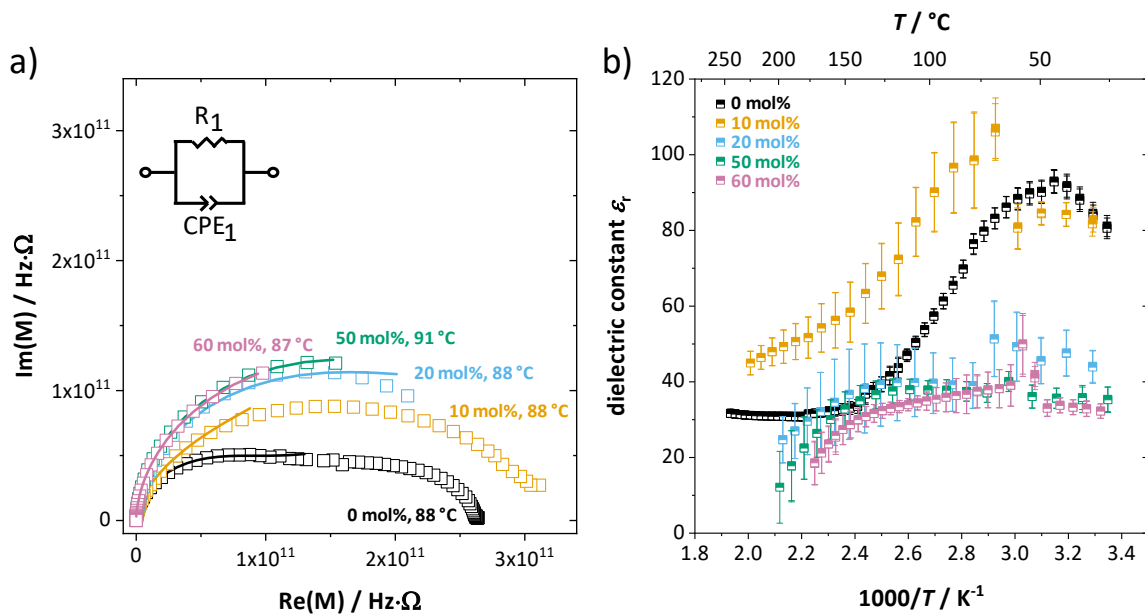


Figure S10: a) Complex modulus (87-91 °C) and b) dielectric constant ϵ_r of anhydrous Li(SCN) (black) and various reaction products of two-phase samples containing Li(SCN) and x $\text{Mg}(\text{SCN})_2$ ($x = 10$ (orange), 20 (blue), 50 (green) or 60 (pink) mol%). The impedance data was fit with the shown equivalent circuit in the respective frequency range.

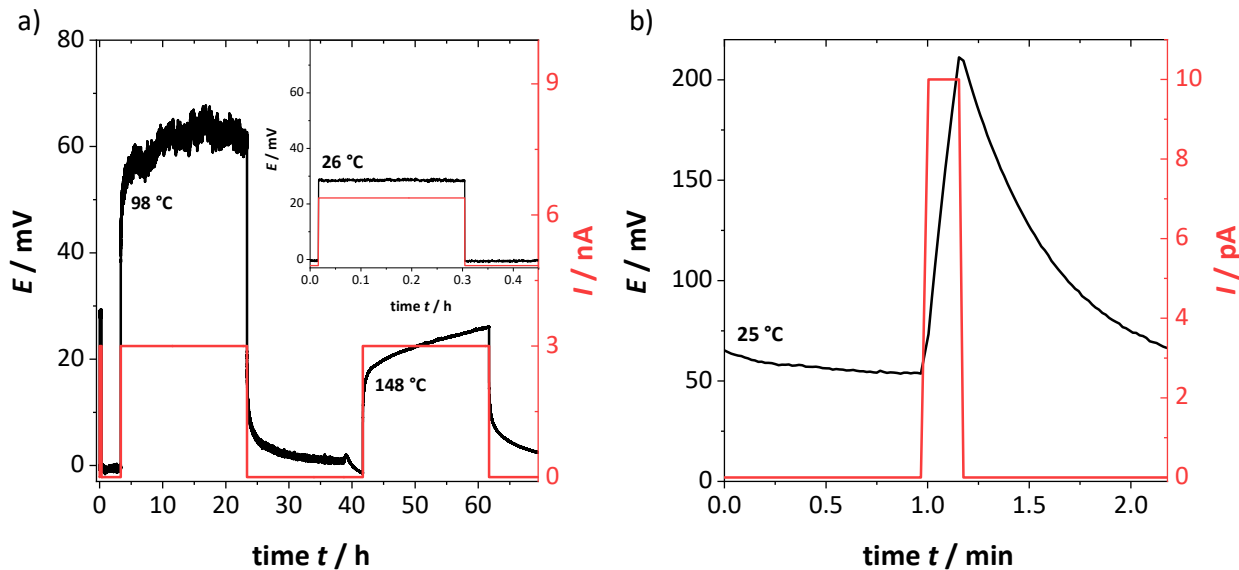


Figure S11: DC measurements of a) Li(SCN) doped with 1.5 mol% $\text{Co}(\text{SCN})_2$ and b) Li(SCN) doped with 1.5 mol% $\text{Zn}(\text{SCN})_2$ at 25 °C. In both cases lithium blocking ruthenium electrodes were employed (as for undoped Li(SCN) in Figure S8a).

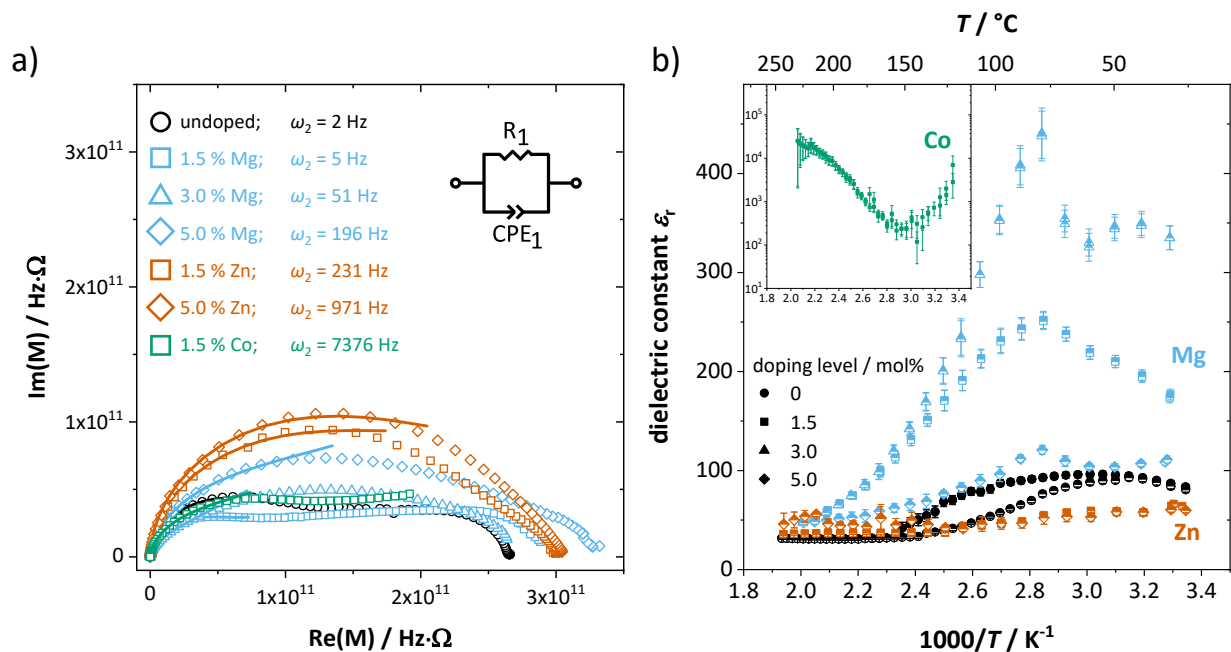


Figure S12: a) Complex modulus (68-69 °C) and b) dielectric constant ϵ_r of undoped (black), Mg^{2+} -doped (blue), Zn^{2+} -doped (red) and Co^{2+} -doped (green) $\text{Li}(\text{SCN})$. The presented data correspond to the low frequency signal termed ω_2 , with the respective peak frequencies as well as the corresponding circuit for fitting shown in (a). Full symbols are heating runs; half-filled symbols are cooling runs.

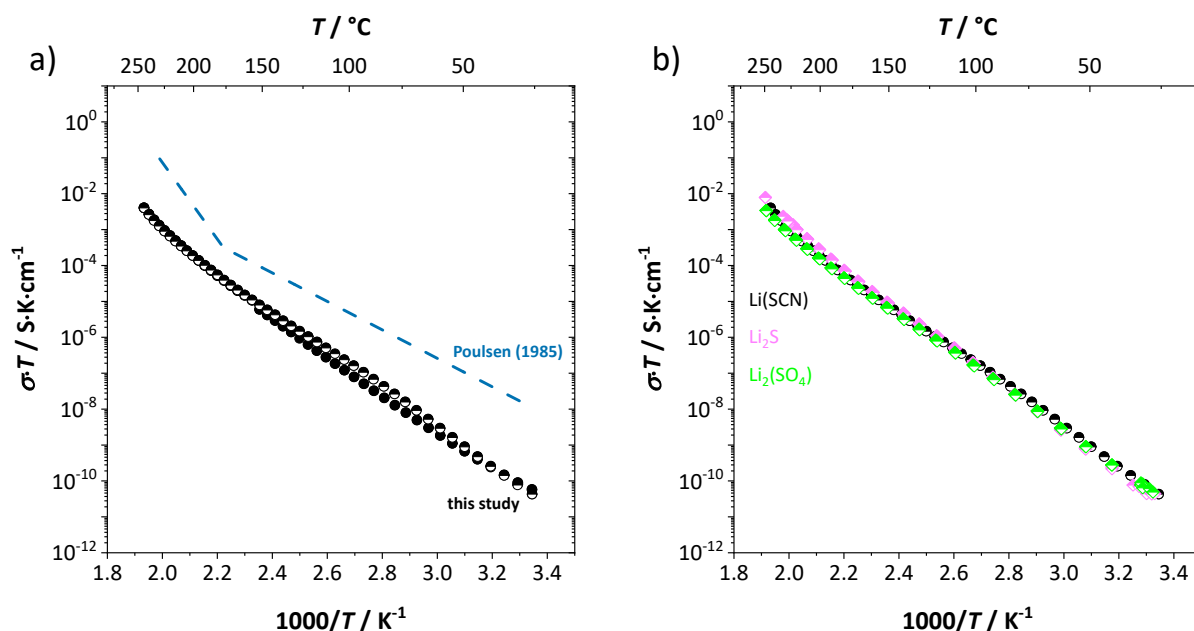


Figure S13: a) Comparison of the measured conductivities in this study (black circles) with the values reported in 1985 by Poulsen (blue, dashed line).¹ b) Measured conductivities of attempted $\text{Li}(\text{SCN})$ acceptor doping with 5.0 mol% of either Li_2S or $\text{Li}_2(\text{SO}_4)$. Full symbols correspond to the heating runs, half-filled symbols to the cooling runs.

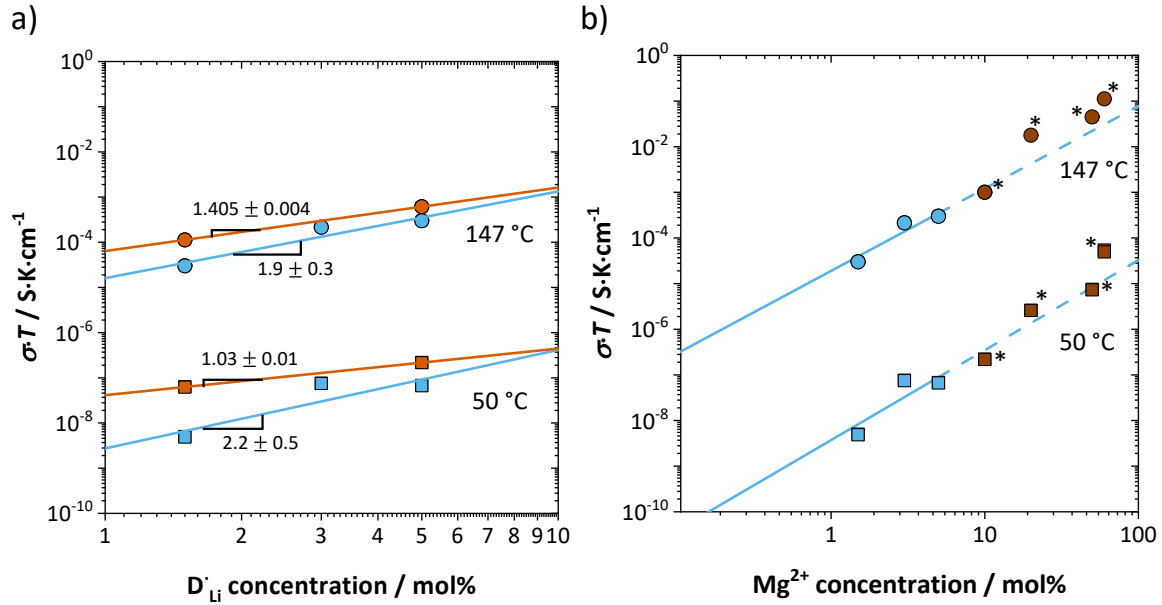


Figure S14: Measured conductivities as a function of donor dopant D_{Li} for Mg^{2+} (blue) and Zn^{2+} (red) at 50 °C (squares) and 147 °C (circles). a) Pure phase samples within the solubility limits of Mg and Zn in Li(SCN). The flattening of the increase in conductivity at 5 mol% dopant concentration could indicate that the solubility limit is actually lower at 3 mol%. b) Inclusion of composites of Li(SCN) and $\text{Mg}_{1.02}\text{Li}_{3.96}(\text{SCN})_6$ (dark red) marked with an asterisk (same slopes as shown in a).

References

- 1 F. W. Poulsen, *Acta Chem. Scand.*, 1985, **A39**, 290–292.
- 2 M. Joos, M. Conrad, R. Merkle, Th. Schleid, J. Maier, R. E. Dinnebier and S. Bette, *Dalton Trans.*, 2021, **50**, 6949–6991.
- 3 J. Dost, *Z. Phys. Chem.*, 1964, **236**, 145–150.
- 4 K. Kynev and R. Dafinowa, *Compt. rend. Acad. Bulg.*, 1967, **20**, 939–942.
- 5 L. A. Aslanov, V. M. Ionov and K. Kynev, *Kristallografiya*, 1976, **21**, 1198–1199.
- 6 New Jersey Zinc Company, *Private Communication*, Palmerton, Pennsylvania, USA.
- 7 M. Joos, University of Stuttgart, 2021.
- 8 A. A. Coelho, *J. Appl. Crystallogr.*, 2018, **51**, 210–218.
- 9 A. A. Coelho, *J. Appl. Crystallogr.*, 2003, **36**, 86–95.
- 10 J. L. F. A. Le Bail, H. Duroy, *Mater. Res. Bull.*, 1988, **23**, 447–452.

- 11 R. W. Cheary and A. Coelho, *J. Appl. Crystallogr.*, 1992, **25**, 109–121.
- 12 R. W. Cheary, A. A. Coelho and J. P. Cline, *J. Res. Natl. Inst. Stand. Technol.*, 2004, **109**, 1–25.
- 13 O. Reckeweg, A. Schulz, B. Blaschkowski, Th. Schleid and F. J. DiSalvo, *Z. Naturforsch.*, 2014, **69b**, 17–24.
- 14 A. A. Coelho, *J. Appl. Crystallogr.*, 2000, **33**, 899–908.
- 15 V. Favre-Nicolin and R. Černý, *Mater. Sci. Forum*, 2004, **443–444**, 35–38.
- 16 H. M. Rietveld, *J. Appl. Crystallogr.*, 1969, **2**, 65–71.
- 17 M. E. Orazem and B. Tribollet, *Electrochemical Impedance Spectroscopy*, John Wiley & Sons, 2011, 2008, vol. 48.
- 18 G. Kresse and J. Furthmüller, *Phys. Rev. B*, 1996, **54**, 11169–11186.
- 19 G. Kresse and J. Furthmüller, *Comput. Mater. Sci.*, 1996, **6**, 15–50.
- 20 P. E. Blöchl, *Phys. Rev. B*, 1994, **50**, 17953–17979.
- 21 G. Kresse and D. Joubert, *Phys. Rev. B Condens. Mater.*, 1999, **59**, 1758–1775.
- 22 J. P. Perdew, K. Burke and M. Ernzerhof, *Phys. Rev. Lett.*, 1996, **77**, 3865–3868.
- 23 J. Heyd, G. E. Scuseria and M. Ernzerhof, *J. Chem. Phys.*, 2003, **118**, 8207–8215.
- 24 A. V. Krukau, O. A. Vydrov, A. F. Izmaylov and G. E. Scuseria, *J. Chem. Phys.*, 2006, **125**, 224106.
- 25 K. Okhotnikov, T. Charpentier and S. Cadars, *J. Cheminformatics*, 2016, **8**, 1–15.
- 26 C. Freysoldt, J. Neugebauer and C. G. Van De Walle, *Phys. Rev. Lett.*, 2009, **102**, 1–4.
- 27 C. Freysoldt, J. Neugebauer and C. G. Van de Walle, *Phys. Status Solidi B Basic Res.*, 2011, **248**, 1067–1076.
- 28 J. Saha and J. Podder, *J. Bangladesh Acad. Sci.*, 1970, **35**, 203–210.
- 29 R. D. Shannon, *Acta Crystallogr.*, 1976, **A32**, 751–767.
- 30 C. J. Wen, B. A. Boukamp, R. A. Huggins and W. Weppner, *J. Electrochem. Soc.*, 1979, **126**, 2258.